Eidgenössische Technische Hochschule Zürich

Ecole polytechnique fédérale de Zurich
Politecnico federale di Zurigo
Swiss Federal Institute of Technology Zurich

Constraint preserving schemes using potential-based fluxes
II. Genuinely multi-dimensional central schemes for systems of conservation laws

S. Mishra and E. Tadmor*

Research Report No. 2009-32
November 2009

Seminar für Angewandte Mathematik
Eidgenössische Technische Hochschule
CH-8092 Zürich
Switzerland

*Department of Mathematics, Institute for Physical Sciences and Technology (IPST), University of Maryland, College Park, MD 20742-4015, USA

CONSTRAINT PRESERVING SCHEMES USING POTENTIAL-BASED FLUXES. II. GENUINELY MULTI-DIMENSIONAL CENTRAL SCHEMES FOR SYSTEMS OF CONSERVATION LAWS.

SIDDHARTHA MISHRA AND EITAN TADMOR

Abstract. We propose an alternative framework for designing genuinely multi-dimensional (GMD) finite volume schemes for systems of conservation laws in two space dimensions. The approach is based on reformulating edge centered numerical fluxes in terms of *vertex centered potentials*. *Any* consistent numerical flux can be used in defining the potentials. Suitable choices of potentials result in schemes that preserve discrete forms of interesting constraints like vorticity and divergence. The schemes are very simple to code, robust and have low computational costs. Numerical examples for scalar conservation laws, system wave equations and Euler equations of gas dynamics are presented to illustrate the efficiency of the schemes.

1. Introduction

We are concerned with hyperbolic system of conservation laws in two space dimensions:

$$\mathbf{U}_t + \mathbf{f}(\mathbf{U})_x + \mathbf{g}(\mathbf{U})_y = 0, \quad (x,y,t) \in \mathbb{R}\times\mathbb{R}\times\mathbb{R}_+, \tag{1.1}$$

where $\mathbf{U}$ is the vector of unknowns and $\mathbf{f}, \mathbf{g}$ are the flux vectors in the x- and y- directions, respectively. Examples for (1.1) include the Euler equations of gas dynamics, the shallow water equations of oceanography, the ideal Magneto-HydroDynamics (MHD) equations of plasma physics and the equations of non-linear elasticity.

It is well known that solutions of (1.1) develop discontinuities in the form of shock waves, even for smooth initial data. Hence, the solutions of (1.1) are sought in a weak sense. Weak solutions are not necessarily unique and (1.1) has to be supplemented with additional admissibility criteria, the so-called *entropy conditions*, [8]. The existence and uniqueness theory for multi-dimensional single conservation laws and for some special cases of one dimensional systems is well developed. The theory for multi-dimensional systems of conservation laws is still in a very primitive stage of development.

It is not possible to obtain explicit formulas for solutions of (1.1), except in the simplest cases. Consequently, numerical methods are heavily used. Among the most popular numerical methods, are the finite volume methods, see [20, 36] for a detailed description. In a finite volume approximation, the computational domain is discretized into cells and an integral form of the conservation law (1.1) is discretized on each cell. This method relies on constructing suitable numerical fluxes in the normal direction, across each cell interface. For simplicity, we consider a uniform Cartesian mesh with mesh sizes $\Delta x, \Delta y$ in the x- and y- directions respectively. It consists of the discrete cells, $\mathcal{C}_{i,j} = [x_{i-\frac{1}{2}}, x_{i+\frac{1}{2}}) \times [y_{j-\frac{1}{2}}, y_{j+\frac{1}{2}})$, centered at the mesh points $(x_i, y_j) = (i\Delta x, j\Delta y),\ (i,j) \in \mathbb{Z}^2$. The cell average of $\mathbf{U}$ over $\mathcal{C}_{i,j}$ (at time t), denoted as $\mathbf{U}_{i,j}(t)$, is updated with the semi-discrete scheme [20, 36]:

$$\frac{d}{dt}\mathbf{U}_{\mathbf{i,j}} = -\frac{1}{\Delta x}(\mathbf{F}_{i+\frac{1}{2},j} - \mathbf{F}_{i-\frac{1}{2},j}) - \frac{1}{\Delta y}(\mathbf{G}_{i,j+\frac{1}{2}} - \mathbf{G}_{i,j-\frac{1}{2}}). \tag{1.2}$$

Date: November 10, 2009.

1991 *Mathematics Subject Classification.* 65M06,35L65.

Key words and phrases. multidimensional evolution equations, nonlinear conservation laws, constraint transport, central difference schemes, potential-based fluxes.

Acknowledgment. The work on this paper was started when S.M. visited the Center of Scientific Computation and Mathematical Modeling (CSCAMM) and he thanks CSCAMM and all its members for the excellent hospitality and facilities. E. T. Research was supported in part by NSF grant 07-07949 and ONR grant N00014-91-J-1076.

The time dependence of all the quantities in the above expression is suppressed for notational convenience. The numerical fluxes are of the form:

$$(\mathbf{F}_{i+\frac{1}{2},j}, \mathbf{G}_{i,j+\frac{1}{2}}) = (\mathbf{F}(\mathbf{U}_{i,j}, \mathbf{U}_{i+1,j}), \mathbf{G}(\mathbf{U}_{i,j}, \mathbf{U}_{i,j+1}))\,.$$

The scheme (1.2) can be extended to higher order of accuracy by employing standard central,[18], and (W) ENO type reconstructions, [16],[32]. The time integration is performed with either the forward Euler method or any standard higher order Runge-Kutta method.

Despite their considerable success, finite volume schemes (1.2) are known to be deficient, [20], in resolving genuinely multi-dimensional waves in the solution of (1.1). The numerical fluxes $\mathbf{F}_{i+\frac{1}{2},j}, \mathbf{G}_{i,j+\frac{1}{2}}$ are defined in each normal direction and lack explicit transverse information. This could result in poor approximation of genuinely multi-dimensional waves. Considerable effort has been devoted to devising *genuinely multi-dimensional* (GMD) finite volume schemes for approximating (1.1). We provide a very brief summary of some of the available methods:

(i.) *Dimensional splitting.* This procedure is based on sequentially updating the cell average in each direction. Second order accuracy results from Strang splitting, [20]. Despite the splitting, the resulting method may still fail to resolve genuinely multi-dimensional waves, [21].

(ii.) *Multi-dimensional wave propagation.* This method is based on the Corner Transport Upwind (CTU) method, [7], for linear equations. Contributions from waves in the transverse direction are explicitly calculated. It was extended to non-linear systems in [21] by solving transverse Riemann problems. The method is implemented in the *CLAWPACK* software package, [20]. A related scheme was proposed in [5].

(iii.) *Method of Transport.* In [12, 13, 29], the non-linear conservation law (1.1) is reformulated locally as a system of transport equations. Explicit solution formulas for the transport equations define a genuinely multi-dimensional scheme. Complicated formulas for specific wave models may be a major disadvantage of this method.

(iv.) *Finite volume Evolution Galerkin (FVEG) methods.* In [22, 23], the conservation law (1.1) is linearized locally and the resulting system is solved in terms of bi-characteristics. The evolution operator defines genuinely multi-dimensional finite volume fluxes by a Galerkin type approximation. The task of deriving explicit solutions in terms of bi-characteristics for specific models may be quite complicated.

(v.) *Residual distribution/Fluctuation-splitting schemes.* Genuinely multi-dimensional methods for unstructured meshes were proposed in [10, 1, 28]. They involve computing a cell residual at each time step and distributing it to the cell nodes by using some suitable upwinding procedure.

The absence of an optimal strategy for genuinely multi-dimensional schemes leaves room for designing a stable GMD scheme that is easy to formulate and code, and has a low computational cost. We present such a scheme in this paper.

A related issue that comes up in the numerical approximation of multi-dimensional conservation laws is the fact that many interesting multi-dimensional systems of conservation laws are augmented with *intrinsic constraints*. Examples include the MHD equations of plasma physics. Solutions of the MHD equations satisfy the constraint that the magnetic field is divergence free, [39]. Another example is provided by the system of wave equations in two space dimensions, [27]:

$$\begin{aligned} p_t + cu_x + cu_y &= 0, \\ u_t + cp_x &= 0, \\ v_t + cp_y &= 0, \end{aligned} \tag{1.3}$$

where c is a given (constant) advection velocity. A straightforward calculation shows that the vorticity, $w = v_x - u_y$, is preserved, i.e,

$$\omega_t \equiv 0. \tag{1.4}$$

Constraints like vorticity and divergence involve the *geometric* interaction of both normal and transverse components of the solution. They reflect the genuinely multi-dimensional structure of the equation (1.1). The standard finite volume scheme (1.2) lacks explicit transverse information. Consequently, it is not surprising

that the scheme (1.2) does not preserve a discrete version of the constraint, leading to numerical instabilities, [39].

A wide variety of numerical methods have been proposed to handle constraints in multi-dimensional conservation laws. These include projection methods, [4, 6], methods that add source terms, [30, 14], and constraint transport methods based on staggering, [3, 9, 17, 27, 31, 37, 38, 2]. These methods are compared extensively in [39]. A detailed summary of these methods can be checked from the introduction of [25].

In a recent paper [25], we proposed a family of finite volume schemes for conservation laws with intrinsic constraints. These schemes were based on reformulating edge-centered numerical fluxes in terms of vertex-centered *potentials*. The family of such schemes is very rich and any consistent numerical flux can define the potential. These potential based schemes were illustrated on the linear magnetic induction equations. It was shown that preserving the constraint (divergence in the case of the induction equations) led to considerably better numerical results than the standard schemes. The schemes were also extremely easy to code and had low computational costs. Furthermore, the potential based schemes proposed in [25] were genuinely multi-dimensional and incorporated explicit transverse information.

Given the deep connection between the genuinely multi-dimensional structure of (1.1) and the preservation of constraints, it is natural to seek a numerical scheme that respects the genuinely multi-dimensional structure of the equations. Furthermore, the scheme should preserve a discrete version of the constraint that may augment the conservation law.

Our starting point is the potential based framework of [25]. This framework can be extended to device a family of GMD schemes for the conservation law (1.1). The schemes are based on the vertex-centered potentials. The class of potential based schemes is very rich. A particular version of the GMD scheme is shown to be entropy stable. Numerical experiments with multi-dimensional scalar conservation laws and the Euler equations of gas dynamics are presented.

A suitable choice of the numerical potential results in a scheme that preserves a discrete version of the intrinsic constraint. The system wave equation (1.3) is considered in detail and numerical experiments highlighting the computational efficiency and constraint preserving abilities of the GMD scheme are described. The *potential* based GMD framework provides a simple, computationally cheap and stable recipe for modifying *any* standard finite volume scheme (1.2) in-order to resolve genuinely multi-dimensional waves and to preserve constraints.

The rest of the paper is organized as follows: in Section 2, the GMD schemes are defined. Entropy stability analysis is carried out in Section 3. Numerical examples for scalar equations and the Euler equations of gas dynamics are described in Sections 4 and 5 respectively. Section 6 deals with constraint preserving GMD schemes and numerical experiments for the system wave equation are described in Section 7.

This paper is the second in a series of papers devoted to numerical schemes for multi-dimensional systems of conservation laws. The first paper, [25], focused on potential based schemes for evolution equations with constraints. This paper concentrates on the genuinely multi-dimensional aspect of these potential based schemes. It also highlights the interplay between the GMD structure of the schemes and preservation of a discrete version of the intrinsic constraint, thus extending the results of [25] to a more general context. The third paper in this series, [26], deals with constraint preserving potential based schemes for the MHD equations.

2. GMD schemes

Following the presentation of [25], we introduce the *numerical potentials* $\phi_{i+\frac{1}{2},j+\frac{1}{2}}$ and $\psi_{i+\frac{1}{2},j+\frac{1}{2}}$ at each vertex $(x_{i+\frac{1}{2}}, y_{j+\frac{1}{2}})$, with the sole requirement that these potentials are consistent with the differential fluxes, i.e,

$$\phi_{i+\frac{1}{2},j+\frac{1}{2}}(\mathbf{U},\cdots,\mathbf{U}) = \mathbf{f}(\mathbf{U}), \quad \psi_{i+\frac{1}{2},j+\frac{1}{2}}(\mathbf{U},\cdots,\mathbf{U}) = \mathbf{g}(\mathbf{U}).$$

We need the following notation for standard averaging and difference operators,

$$\begin{aligned} \mu_x a_{I,J} &:= \frac{a_{I+\frac{1}{2},J} + a_{I-\frac{1}{2},J}}{2}, \quad \mu_y a_{I,J} := \frac{a_{I,J+\frac{1}{2}} + a_{I,J-\frac{1}{2}}}{2}, \\ \delta_x a_{I,J} &:= \frac{a_{I+\frac{1}{2},J} - a_{I-\frac{1}{2},J}}{\Delta x}, \quad \delta_y a_{I,J} := \frac{a_{I,J+\frac{1}{2}} - a_{I,J-\frac{1}{2}}}{\Delta y}. \end{aligned} \tag{2.1}$$

A word about our notations: we note that the above discrete operators could be used with indexes I, J which are placed at the center or at the edge of the computational cells, e.g., $I = i$ or $I = i + \frac{1}{2}$. In either case, we tag the resulting discrete operators according to the center of their stencil; thus, for example, $\mu_x w_{i+\frac{1}{2}}$ employs grid values placed on the integer-indexed edges, w_i and w_{i+1}, whereas $\delta_y w_j$ employs the half-integer indexed centers, $w_{j\pm\frac{1}{2}}$.

We now set the numerical fluxes:

$$\begin{aligned} \mathbf{F}_{i+\frac{1}{2},j} &= \mu_y \phi_{i+\frac{1}{2},j}, \\ \mathbf{G}_{i,j+\frac{1}{2}} &= \mu_x \phi_{i,j+\frac{1}{2}}. \end{aligned} \tag{2.2}$$

The resulting finite volume scheme written in terms of the numerical potentials reads

$$\begin{aligned} \frac{d}{dt}\mathbf{U}_{i,j} &= -\delta_x \mu_y \phi_{i,j} - \delta_y \mu_x \psi_{i,j}, \\ &= -\frac{1}{\Delta x}\Big(\frac{1}{2}(\phi_{i+\frac{1}{2},j+\frac{1}{2}} + \phi_{i+\frac{1}{2},j-\frac{1}{2}}) - \frac{1}{2}(\phi_{i-\frac{1}{2},j+\frac{1}{2}} + \phi_{i-\frac{1}{2},j-\frac{1}{2}})\Big) \\ &\quad - \frac{1}{\Delta y}\Big(\frac{1}{2}(\psi_{i+\frac{1}{2},j+\frac{1}{2}} + \psi_{i-\frac{1}{2},j+\frac{1}{2}}) - \frac{1}{2}(\psi_{i+\frac{1}{2},j-\frac{1}{2}} + \psi_{i-\frac{1}{2},j-\frac{1}{2}})\Big). \end{aligned} \tag{2.3}$$

The potential based scheme (2.3) is clearly conservative as well as consistent as the potentials ϕ, ψ are consistent. A glimpse of the genuinely multi-dimensional nature of the scheme is evident in the form (2.3). The potentials are differenced in the normal direction but averaged in the transverse direction.

2.1. **The family of potential based schemes is rich.** Standard finite volume fluxes are the *building blocks* of the potential based scheme (2.3). They define the numerical potentials in many different ways. Some of them are outlined below.

2.1.1. *Symmetric potentials.* In this approach, the potentials are defined by averaging the finite volume fluxes neighboring a vertex:

$$\begin{aligned} \phi_{i+\frac{1}{2},j+\frac{1}{2}} &= \mu_y \mathbf{F}_{i+\frac{1}{2},j+\frac{1}{2}}, \\ \psi_{i+\frac{1}{2},j+\frac{1}{2}} &= \mu_x \mathbf{G}_{i+\frac{1}{2},j+\frac{1}{2}}, \end{aligned} \tag{2.4}$$

for any standard numerical fluxes $\mathbf{F}, \mathbf{G}$ consistent with $\mathbf{f}$ and $\mathbf{g}$ respectively. An explicit computation of (2.3) with potentials (2.4) leads to the revealing form,

$$\begin{aligned} \frac{d}{dt}\mathbf{U}_{i,j} = &-\frac{1}{2\Delta x}(\mu_y \mathbf{F}_{i+\frac{1}{2},j+\frac{1}{2}} + \mu_y \mathbf{F}_{i+\frac{1}{2},j-\frac{1}{2}} - \mu_y \mathbf{F}_{i-\frac{1}{2},j+\frac{1}{2}} - \mu_y \mathbf{F}_{i-\frac{1}{2},j-\frac{1}{2}}) \\ &- \frac{1}{2\Delta y}(\mu_x \mathbf{G}_{i+\frac{1}{2},j+\frac{1}{2}} + \mu_x \mathbf{G}_{i-\frac{1}{2},j+\frac{1}{2}} - \mu_x \mathbf{G}_{i+\frac{1}{2},j-\frac{1}{2}} - \mu_x \mathbf{G}_{i-\frac{1}{2},j-\frac{1}{2}}). \end{aligned} \tag{2.5}$$

Comparing the potential based scheme (2.5) with the standard finite volume scheme (1.2), we observe that the potential based scheme modifies (1.2) by averaging the fluxes in the transverse direction. Hence, it incorporates *explicit* transverse information in each direction. The local stencil for the GMD scheme (2.5) consists of nine points instead of the standard five point stencil for the finite volume scheme (1.2).

2.1.2. *Weighted symmetric potentials.* Weighted averages of the neighboring fluxes can be considered in place of the simple averaging used in (2.4). Let $0 \le \alpha_{i+\frac{1}{2},j+\frac{1}{2}}, \beta_{i+\frac{1}{2},j+\frac{1}{2}} \le 1$ be weights, then the weighted potential is defined as

$$\begin{aligned} \phi_{i+\frac{1}{2},j+\frac{1}{2}} &= \alpha_{i+\frac{1}{2},j+\frac{1}{2}} \mathbf{F}_{i+\frac{1}{2},j+1} + (1 - \alpha_{i+\frac{1}{2},j+\frac{1}{2}}) \mathbf{F}_{i+\frac{1}{2},j}, \\ \psi_{i+\frac{1}{2},j+\frac{1}{2}} &= \beta_{i+\frac{1}{2},j+\frac{1}{2}} \mathbf{G}_{i+1,j+\frac{1}{2}} + (1 - \beta_{i+\frac{1}{2},j+\frac{1}{2}}) \mathbf{G}_{i,j+1/2}. \end{aligned} \tag{2.6}$$

The weights are chosen, based on the local characteristic speeds. A particular choice depends on the Jacobian matrices,

$$A_{i+\frac{1}{2},j+\frac{1}{2}} = \partial_{\mathbf{U}} \mathbf{f}(\mu_y \mu_x \mathbf{U}_{i+\frac{1}{2},j+\frac{1}{2}}), \quad B_{i+\frac{1}{2},j+\frac{1}{2}} = \partial_{\mathbf{U}} \mathbf{g}(\mu_x \mu_y \mathbf{U}_{i+\frac{1}{2},j+\frac{1}{2}}).$$

Denote the eigenvalues of A and B by λ_l^x, λ_l^y for $l = 1, 2, \cdots, N$. Then a simple choice of weights is

$$\begin{aligned}\alpha_{i+\frac{1}{2},j+\frac{1}{2}} &= \frac{\max\{-(\lambda_1^y)_{i+\frac{1}{2},j+\frac{1}{2}}, 0\}}{\max\{-(\lambda_1^y)_{i+\frac{1}{2},j+\frac{1}{2}}, 0\} + \max\{(\lambda_N^y)_{i+\frac{1}{2},j+\frac{1}{2}}, 0\}},\\ \beta_{i+\frac{1}{2},j+\frac{1}{2}} &= \frac{\max\{-(\lambda_1^x)_{i+\frac{1}{2},j+\frac{1}{2}}, 0\}}{\max\{-(\lambda_1^x)_{i+\frac{1}{2},j+\frac{1}{2}}, 0\} + \max\{(\lambda_N^x)_{i+\frac{1}{2},j+\frac{1}{2}}, 0\}}.\end{aligned} \tag{2.7}$$

This choice of weights implies that the potential (2.6) is "upwinded".

2.1.3. *Staggered symmetric potentials.* We can also define the potential as

$$\phi_{i+\frac{1}{2},j+\frac{1}{2}} = \mathbf{F}(\mu_y \mathbf{U}_{i,j+\frac{1}{2}}, \mu_y \mathbf{U}_{i+1,j+\frac{1}{2}}), \quad \psi_{i+\frac{1}{2},j+\frac{1}{2}} = \mathbf{G}(\mu_x \mathbf{U}_{i+\frac{1}{2},j}, \mu_x \mathbf{U}_{i+\frac{1}{2},j+1}) \tag{2.8}$$

for any consistent numerical fluxes $\mathbf{F}, \mathbf{G}$.

2.1.4. *Diagonal potentials.* Define the *diagonal* fluxes,

$$\begin{aligned}\mathbf{F}^+_{i+\frac{1}{2},j+\frac{1}{2}} &= \mathbf{F}(\mathbf{U}_{i,j}, \mathbf{U}_{i+1,j+1}), \quad \mathbf{G}^+_{i+\frac{1}{2},j+\frac{1}{2}} &&= \mathbf{G}(\mathbf{U}_{i,j}, \mathbf{U}_{i+1,j+1}),\\ \mathbf{F}^-_{i+\frac{1}{2},j-\frac{1}{2}} &= \mathbf{F}(\mathbf{U}_{i,j}, \mathbf{U}_{i+1,j-1}), \quad \mathbf{G}^-_{i-\frac{1}{2},j+\frac{1}{2}} &&= \mathbf{G}(\mathbf{U}_{i,j}, \mathbf{U}_{i-1,j+1}),\end{aligned} \tag{2.9}$$

for any two numerical fluxes $\mathbf{F}, \mathbf{G}$, consistent with $\mathbf{f}$ and $\mathbf{g}$ respectively. Note that the *diagonal* fluxes $\mathbf{F}^\pm, \mathbf{G}^\pm$ amount to rotating the axes by angles of $\frac{\pi}{4}$ and $-\frac{\pi}{4}$ respectively

The diagonal fluxes (2.9) are used to define the diagonal potentials, see [25]:

$$\begin{aligned}\phi_{i+\frac{1}{2},j+\frac{1}{2}} &= \frac{1}{2}(F^+_{i+\frac{1}{2},j+\frac{1}{2}} + F^-_{i+\frac{1}{2},j+\frac{1}{2}}),\\ \psi_{i+\frac{1}{2},j+\frac{1}{2}} &= \frac{1}{2}(G^+_{i+\frac{1}{2},j+\frac{1}{2}} + G^-_{i+\frac{1}{2},j+\frac{1}{2}}).\end{aligned} \tag{2.10}$$

The potential based scheme (2.3) with any of the above choices of potential is very robust in all numerical experiments. The differences in numerical results for different choices of the potentials are minor. Hence, we focus on the symmetric potential (2.4) and the resulting, symmetric GMD scheme (2.5) in the sequel.

However, we are unable to prove non-linear stability of the above potential based schemes. This motivates us to modify them slightly and propose another class of potential based schemes.

2.2. **Isotropic GMD scheme.** Instead of using (2.2) to define the fluxes, we set them as

$$\begin{aligned}\widetilde{F}_{i+\frac{1}{2},j} &= \frac{1}{4}(\mathbf{F}^+_{i+\frac{1}{2},j+\frac{1}{2}} + 2\mathbf{F}_{i+\frac{1}{2},j} + \mathbf{F}^-_{i+\frac{1}{2},j-\frac{1}{2}}),\\ \widetilde{G}_{i,j+\frac{1}{2}} &= \frac{1}{4}(\mathbf{G}^+_{i+\frac{1}{2},j+\frac{1}{2}} + 2\mathbf{G}_{i,j+\frac{1}{2}} + \mathbf{G}^-_{i-\frac{1}{2},j+\frac{1}{2}}),\end{aligned} \tag{2.11}$$

for any two consistent finite volume fluxes $\mathbf{F}, \mathbf{G}$ and their corresponding diagonal fluxes (2.9). The resulting finite volume scheme reads as

$$\begin{aligned}\frac{d}{dt}\mathbf{U}_{i,j} &= -\delta_x \widetilde{\mathbf{F}}_{i,j} - \delta_y \widetilde{\mathbf{G}}_{i,j},\\ &= -\frac{1}{4\Delta x}\left(\Delta_/ \mathbf{F}^+_{i,j} + 2\Delta_x \mathbf{F}_{i,j} + \Delta_\backslash F^-_{i,j}\right) - \frac{1}{4\Delta y}\left(\Delta_/ \mathbf{G}^+_{i,j} + 2\Delta_y \mathbf{G}_{i,j} - \Delta_\backslash G^-_{i,j}\right),\end{aligned} \tag{2.12}$$

where we have used the undivided *diagonal* difference operators:

$$\Delta_/ a_{I,J} = a_{I+\frac{1}{2},J+\frac{1}{2}} - a_{I-\frac{1}{2},J-\frac{1}{2}}, \quad \Delta_\backslash a_{I,J} = a_{I+\frac{1}{2},J-\frac{1}{2}} - a_{I-\frac{1}{2},J+\frac{1}{2}}, \tag{2.13}$$

and

$$\Delta_x = \Delta x \delta_x, \quad \Delta_y = \Delta y \delta_y,$$

denote the undivided difference operators.

The GMD structure of the scheme is clearly visible in (2.12). The scheme averages the fluxes along transverse directions. In contrast to the symmetric scheme (2.5), we observe that the transverse information in (2.12) is obtained by "rotating" the fluxes. Since the scheme (2.12) takes into account all the directions in a cell, we term it as the *isotropic* GMD scheme.

2.3. **Choice of numerical fluxes.** The symmetric GMD scheme (2.5) and the isotropic GMD scheme (2.12) need to be completed by specifying the *building block* numerical fluxes $\mathbf{F}, \mathbf{G}$. A key advantage of our approach is that *any* consistent numerical fluxes $\mathbf{F}, \mathbf{G}$ can be used. A simple choice is the Rusanov flux. Let $(\mathbf{A}, \mathbf{B}) = (\partial_{\mathbf{U}}\mathbf{f}, \partial_{\mathbf{U}}\mathbf{g})$ be the flux Jacobians and $\lambda^x_{\max}$ and $\lambda^y_{\max}$ be the maximum eigenvalues of $\mathbf{A}$ and $\mathbf{B}$ respectively, for a given state. Then the Rusanov flux ([18]) is

$$\begin{aligned} \mathbf{F}_{i+\frac{1}{2},j} &= \frac{1}{2}(\mathbf{f}_{i,j} + \mathbf{f}_{i+1,j} - \max\{|(\lambda^x_{\max})_{i,j}|, |(\lambda^x_{\max})_{i+1,j}|\}(\mathbf{U}_{i+1,j} - \mathbf{U}_{i,j})), \\ \mathbf{G}_{i,j+\frac{1}{2}} &= \frac{1}{2}(\mathbf{g}_{i,j} + \mathbf{g}_{i,j+1} - \max\{|(\lambda^y_{\max})_{i,j}|, |(\lambda^y_{\max})_{i,j+1}|\}(\mathbf{U}_{i,j+1} - \mathbf{U}_{i,j})). \end{aligned} \tag{2.14}$$

Note that the only characteristic information in the Rusanov flux is a local estimate on the wave speeds. This flux is almost Jacobian free and is very simple to implement. It has a very low computational cost.

2.4. **Second-order schemes.** The order of accuracy of the schemes (2.5) and (2.12) are related to the choice of numerical fluxes $\mathbf{F}, \mathbf{G}$. A non-oscillatory piecewise bilinear reconstruction in each cell defines a second-order accurate scheme. For simplicity, we use the reconstruction proposed in [18].

2.4.1. *Second-Order non-oscillatory reconstruction.* In each cell $\mathcal{C}_{i,j}$, the cell averages $\mathbf{U}_{i,j}$ are used to define the piecewise bilinear component wise reconstruction:

$$\mathbf{p}_{i,j}(x,y) = \mathbf{U}_{i,j} + \frac{\mathbf{U}'_{i,j}}{\Delta x}(x - x_i) + \frac{\mathbf{U}^{\backprime}_{i,j}}{\Delta y}(y - y_j). \tag{2.15}$$

The numerical derivatives are

$$\begin{aligned} \mathbf{U}'_{i,j} &= \text{minmod}(\mathbf{U}_{i+1,j} - \mathbf{U}_{i,j}, 0.5(\mathbf{U}_{i+1,j} - \mathbf{U}_{i-1,j}), \mathbf{U}_{i,j} - \mathbf{U}_{i-1,j}), \\ \mathbf{U}^{\backprime}_{i,j} &= \text{minmod}(\mathbf{U}_{i,j+1} - \mathbf{U}_{i,j}, 0.5(\mathbf{U}_{i,j+1} - \mathbf{U}_{i,j-1}), \mathbf{U}_{i,j} - \mathbf{U}_{i,j-1}). \end{aligned} \tag{2.16}$$

The minmod function is defined as

$$\begin{aligned} \text{minmod}(a,b,c) &= sgn(a)\min\{|a|, |b|, |c|\}, \quad \text{if} \quad sgn(a) = sgn(b) = sgn(c), \\ &= 0, \qquad \text{otherwise.} \end{aligned}$$

The limiter ensures that the reconstruction of each unknown is TVD. We need the corner point values of the reconstructed polynomial in each cell,

$$\mathbf{U}^E_{i,j} = \mathbf{p}_{i,j}(x_{i+\frac{1}{2}}, y_j), \quad \mathbf{U}^W_{i,j} = \mathbf{p}_{i,j}(x_{i-\frac{1}{2}}, y_j), \quad \mathbf{U}^N_{i,j} = \mathbf{p}_{i,j}(x_i, y_{j+\frac{1}{2}}), \quad \mathbf{U}^S_{i,j} = \mathbf{p}_{i,j}(x_i, y_{j-\frac{1}{2}}),$$
$$\mathbf{U}^{NE}_{i,j} = \mathbf{p}_{i,j}(x_{i+\frac{1}{2}}, y_{j+\frac{1}{2}}), \mathbf{U}^{NW}_{i,j} = \mathbf{p}_{i,j}(x_{i-\frac{1}{2}}, y_{j+\frac{1}{2}}), \quad \mathbf{U}^{SE}_{i,j} = \mathbf{p}_{i,j}(x_{i+\frac{1}{2}}, y_{j-\frac{1}{2}}), \ \mathbf{U}^{SW}_{i,j} = \mathbf{p}_{i,j}(x_{i-\frac{1}{2}}, y_{j-\frac{1}{2}}).$$

Given any two-point fluxes $\mathbf{F}, \mathbf{G}$, the mid-point rule computes a second-order form of the fluxes:

$$\mathbf{F}_{i+\frac{1}{2},j} = \mathbf{F}(\mathbf{U}^E_{i,j}, \mathbf{U}^W_{i+1,j}), \quad \mathbf{G}_{i,j+\frac{1}{2}} = \mathbf{G}(\mathbf{U}^N_{i,j}, \mathbf{U}^S_{i,j+1}). \tag{2.17}$$

Second-order versions of the diagonal fluxes are

$$\begin{aligned} \mathbf{F}^+_{i+\frac{1}{2},j+\frac{1}{2}} &= \mathbf{F}(\mathbf{U}^{NE}_{i,j}, \mathbf{U}^{SW}_{i+1,j+1}), \quad \mathbf{G}^+_{i+\frac{1}{2},j+\frac{1}{2}} = \mathbf{G}(\mathbf{U}^{NE}_{i,j}, \mathbf{U}^{SW}_{i+1,j+1}), \\ \mathbf{F}^-_{i+\frac{1}{2},j-\frac{1}{2}} &= \mathbf{F}(\mathbf{U}^{SE}_{i,j}, \mathbf{U}^{NW}_{i+1,j-1}), \quad \mathbf{G}^-_{i-\frac{1}{2},j+\frac{1}{2}} = \mathbf{G}(\mathbf{U}^{NW}_{i,j}, \mathbf{U}^{SE}_{i-1,j+1}). \end{aligned} \tag{2.18}$$

A second-order accurate version of the GMD schemes is obtained by using the above second-order fluxes.

3. Stability Analysis

The GMD framework is based on the *building blocks*, the standard finite volume fluxes $\mathbf{F}, \mathbf{G}$. If the *building blocks* are stable in a "suitable" sense, then we show that the resulting GMD scheme is stable. The appropriate framework for stability of numerical approximations of the multi-dimensional system of conservation laws (1.1) is the *non-linear entropy stability* framework, introduced in the pioneering papers of Tadmor [33, 34, 35].

We assume that the system (1.1) is equipped with a convex entropy function $\eta(\mathbf{U})$ and compatible entropy fluxes θ, ζ such that solutions of (1.1) satisfy the entropy inequality,

$$\eta_t + \theta_x + \zeta_y \leq 0. \tag{3.1}$$

The above inequality holds in the sense of distributions. The entropy inequality leads to stability estimates for the solution and provides a criteria for selecting physically meaningful solutions, [8].

Let $\mathbf{V}(\mathbf{U}) = \partial_{\mathbf{U}}\eta$ be the vector of entropy variables and $(\sigma, \kappa) = (\langle \mathbf{V}, \mathbf{f}\rangle - \theta, \langle \mathbf{V}, \mathbf{g}\rangle - \zeta)$ the entropy potentials associated with (1.1). The starting point of the entropy stability framework of [34] is the definition:

Definition 3.1. *Entropy conservative fluxes: Numerical fluxes $\mathbf{F}^*_{i+\frac{1}{2},j}, \mathbf{G}^*_{i,j+\frac{1}{2}}$ are termed entropy conservative if they satisfy:*

$$\langle \Delta_x \mathbf{V}_{i+\frac{1}{2},j}, \mathbf{F}^*_{i+\frac{1}{2},j}\rangle = \Delta_x \sigma_{i+\frac{1}{2},j}, \quad \langle \Delta_y \mathbf{V}_{i,j+\frac{1}{2}}, \mathbf{G}^*_{i,j+\frac{1}{2}}\rangle = \Delta_y \kappa_{i,j+\frac{1}{2}}, \tag{3.2}$$

for undivided difference operators $\Delta_{x,y}$.

Entropy conservative fluxes exist ([34]) and can be written down explicitly ([35]). They are used to define

Definition 3.2. *Entropy stable fluxes: We term numerical fluxes $\mathbf{F}_{i+\frac{1}{2},j}, \mathbf{G}_{i,j+\frac{1}{2}}$ entropy stable if they can be written as*

$$\mathbf{F}_{i+\frac{1}{2},j} = \mathbf{F}^*_{i+\frac{1}{2},j} - Q_{i+\frac{1}{2},j}\Delta_x \mathbf{V}_{i+\frac{1}{2},j}, \quad \mathbf{G}_{i,j+\frac{1}{2}} = \mathbf{G}^*_{i,j+\frac{1}{2}} - R_{i,j+\frac{1}{2}}\Delta_y \mathbf{V}_{i,j+\frac{1}{2}} \tag{3.3}$$

for strictly positive definite viscosity matrices Q, R ,i.e,

$$\min_{i,j}\{\langle \mathbf{W}, Q\mathbf{W}\rangle, \langle \mathbf{W}, R\mathbf{W}\rangle\} \geq C\|\mathbf{W}\|^2 \tag{3.4}$$

for any vector $\mathbf{W}$ and some constant C (independent of mesh size).

It was shown in [34] that any finite volume scheme (1.2) with *entropy stable* numerical fluxes $\mathbf{F}, \mathbf{G}$ satisfies a discrete version of the entropy inequality (3.1).

We extend the entropy stability results of [34] to the setting of GMD schemes. For any entropy conservative fluxes, $\mathbf{F}^*$ and $\mathbf{G}^*$ (3.2) for the system (1.1), we can define the corresponding *diagonal* entropy conservative fluxes $\mathbf{F}^{\pm,*}$ and $\mathbf{G}^{\pm,*}$, in analogy with (2.9). The *diagonal* entropy stable fluxes are defined analogously. We have the following stability theorem,

Theorem 3.1. *Let the solution of the system* (1.1) *satisfy the entropy inequality* (3.1)*. Assume that the building block numerical fluxes $\mathbf{F}, \mathbf{G}$, are entropy stable. Then the isotropic GMD scheme* (2.12) *is entropy stable, i.e, approximate solutions $\mathbf{U}_{i,j}$ computed with* (2.12) *satisfy the stability estimate:*

$$\frac{d}{dt}\sum_{i,j}\eta(\mathbf{U}_{i,j}(t)) \leq 0. \tag{3.5}$$

Proof. We modify the approach of [34] to the current setting. We multiply both sides of the isotropic GMD scheme (2.12) by $\mathbf{V}_{i,j}$ to obtain

$$\begin{aligned}\frac{d}{dt}\eta_{i,j} = &-\frac{1}{4\Delta x}\left(\langle \mathbf{V}_{i,j}, \Delta_/ \mathbf{F}^+_{i,j}\rangle + 2\langle \mathbf{V}_{i,j}, \Delta_x \mathbf{F}_{i,j}\rangle + \langle \mathbf{V}_{i,j}, \Delta_\backslash F^-_{i,j}\rangle\right)\\ &-\frac{1}{4\Delta y}\left(\langle \mathbf{V}_{i,j}, \Delta_/ \mathbf{G}^+_{i,j}\rangle + 2\langle \mathbf{V}_{i,j}, \Delta_y \mathbf{G}_{i,j}\rangle - \langle \mathbf{V}_{i,j}, \Delta_\backslash G^-_{i,j}\rangle\right).\end{aligned} \tag{3.6}$$

Denote the first term involving the inner product on the right hand side of (3.6) as

$$T = \langle \mathbf{V}_{i,j}, \Delta_/ \mathbf{F}^+_{i,j}\rangle, \tag{3.7}$$

Substituting the definition (3.3) of an entropy stable flux $\mathbf{F}^+$,

$$T = \underbrace{\langle \mathbf{V}_{i,j}, \Delta_/ \mathbf{F}^{+,*}_{i,j}\rangle}_{T_1} - \underbrace{\left(\langle \mathbf{V}_{i,j}, Q_{i+\frac{1}{2},j+\frac{1}{2}}\Delta_/ \mathbf{V}_{i+\frac{1}{2},j+\frac{1}{2}}\rangle - \langle \mathbf{V}_{i,j}, Q_{i-\frac{1}{2},j-\frac{1}{2}}\Delta_/ \mathbf{V}_{i-\frac{1}{2},j-\frac{1}{2}}\rangle\right)}_{T_2}.$$

We consider the terms T_1 and T_2 separately. Defining the *diagonal* averaging operator:

$$\mu_/ a_{I,J} = \frac{a_{I+\frac{1}{2},J+\frac{1}{2}} + a_{I-\frac{1}{2},J-\frac{1}{2}}}{2}.$$

and using the simple identity:

$$\mathbf{V}_{i,j} = \mu_{/}\mathbf{V}_{i+\frac{1}{2},j+\frac{1}{2}} - \frac{1}{2}\Delta_{/}\mathbf{V}_{i+\frac{1}{2},j+\frac{1}{2}}, \tag{3.8}$$

we obtain,

$$\begin{aligned} T_1 = &\langle \mu_{/}\mathbf{V}_{i+\frac{1}{2},j+\frac{1}{2}}, \mathbf{F}^{+,*}_{i+\frac{1}{2},j+\frac{1}{2}}\rangle - \langle \mu_{/}\mathbf{V}_{i-\frac{1}{2},j-\frac{1}{2}}, \mathbf{F}^{+,*}_{i-\frac{1}{2},j-\frac{1}{2}}\rangle \\ &- \frac{1}{2}\langle \Delta_{/}\mathbf{V}_{i+\frac{1}{2},j+\frac{1}{2}}, \mathbf{F}^{+,*}_{i+\frac{1}{2},j+\frac{1}{2}}\rangle - \frac{1}{2}\langle \Delta_{/}\mathbf{V}_{i-\frac{1}{2},j-\frac{1}{2}}, \mathbf{F}^{+,*}_{i-\frac{1}{2},j-\frac{1}{2}}\rangle. \end{aligned}$$

Entropy conservative flux $\mathbf{F}^{+,*}$ satisfies the relation:

$$\langle \Delta_{/}\mathbf{V}_{i+\frac{1}{2},j+\frac{1}{2}}, \mathbf{F}^{+,*}_{i+\frac{1}{2},j+\frac{1}{2}}\rangle = \Delta_{/}\sigma_{i+\frac{1}{2},j+\frac{1}{2}}.$$

Therefore

$$T_1 = \langle \mu_{/}\mathbf{V}_{i+\frac{1}{2},j+\frac{1}{2}}, \mathbf{F}^{+,*}_{i+\frac{1}{2},j+\frac{1}{2}}\rangle - \langle \mu_{/}\mathbf{V}_{i-\frac{1}{2},j-\frac{1}{2}}, \mathbf{F}^{+,*}_{i-\frac{1}{2},j-\frac{1}{2}}\rangle - \frac{1}{2}\Delta_{/}\sigma_{i+\frac{1}{2},j+\frac{1}{2}} - \frac{1}{2}\Delta_{/}\sigma_{i-\frac{1}{2},j-\frac{1}{2}}.$$

A simple algebraic manipulation yields

$$T_1 = \langle \mu_{/}\mathbf{V}_{i+\frac{1}{2},j+\frac{1}{2}}, \mathbf{F}^{+,*}_{i+\frac{1}{2},j+\frac{1}{2}}\rangle - \langle \mu_{/}\mathbf{V}_{i-\frac{1}{2},j-\frac{1}{2}}, \mathbf{F}^{+,*}_{i-\frac{1}{2},j-\frac{1}{2}}\rangle - \mu_{/}\sigma_{i+\frac{1}{2},j+\frac{1}{2}} + \mu_{/}\sigma_{i-\frac{1}{2},j-\frac{1}{2}}.$$

Using the identity (3.8) in the numerical viscosity term T_2, we obtain

$$\begin{aligned} T_2 = &\langle \mu_{/}\mathbf{V}_{i+\frac{1}{2},j+\frac{1}{2}}, Q_{i+\frac{1}{2},j+\frac{1}{2}}\Delta_{/}\mathbf{V}_{i+\frac{1}{2},j+\frac{1}{2}}\rangle - \langle \mu_{/}\mathbf{V}_{i+\frac{1}{2},j+\frac{1}{2}}, Q_{i-\frac{1}{2},j-\frac{1}{2}}\Delta_{/}\mathbf{V}_{i-\frac{1}{2},j-\frac{1}{2}}\rangle \\ &- \frac{1}{2}\langle \Delta_{/}\mathbf{V}_{i+\frac{1}{2},j+\frac{1}{2}}, Q_{i+\frac{1}{2},j+\frac{1}{2}}\Delta_{/}\mathbf{V}_{i+\frac{1}{2},j+\frac{1}{2}}\rangle - \frac{1}{2}\langle \mu_{/}\mathbf{V}_{i+\frac{1}{2},j+\frac{1}{2}}, Q_{i-\frac{1}{2},j-\frac{1}{2}}\Delta_{/}\mathbf{V}_{i-\frac{1}{2},j-\frac{1}{2}}\rangle. \end{aligned}$$

Let

$$\theta^{+}_{i+\frac{1}{2},j+\frac{1}{2}} = \langle \mu_{/}\mathbf{V}_{i+\frac{1}{2},j+\frac{1}{2}}, \mathbf{F}^{+,*}_{i+\frac{1}{2},j+\frac{1}{2}}\rangle - \mu_{/}\sigma_{i+\frac{1}{2},j+\frac{1}{2}} - \langle \mu_{/}\mathbf{V}_{i+\frac{1}{2},j+\frac{1}{2}}, Q_{i+\frac{1}{2},j+\frac{1}{2}}\Delta_{/}\mathbf{V}_{i+\frac{1}{2},j+\frac{1}{2}}\rangle$$

Using the above definition and calculations, we obtain

$$T = T_1 - T_2 = \Delta_{/}\theta^{+}_{i,j} + \frac{1}{2}\langle \Delta_{/}\mathbf{V}_{i+\frac{1}{2},j+\frac{1}{2}}, Q_{i+\frac{1}{2},j+\frac{1}{2}}\Delta_{/}\mathbf{V}_{i+\frac{1}{2},j+\frac{1}{2}}\rangle + \frac{1}{2}\langle \Delta_{/}\mathbf{V}_{i+\frac{1}{2},j+\frac{1}{2}}, Q_{i-\frac{1}{2},j-\frac{1}{2}}\Delta_{/}\mathbf{V}_{i-\frac{1}{2},j-\frac{1}{2}}\rangle.$$

Entropy stability condition (3.4) implies

$$T \geq \Delta_{/}\theta^{+}_{i,j} + C\left(\|\Delta_{/}\mathbf{V}_{i+\frac{1}{2},j+\frac{1}{2}}\|^2 + \|\Delta_{/}\mathbf{V}_{i-\frac{1}{2},j-\frac{1}{2}}\|^2\right). \tag{3.9}$$

Define the following numerical entropy fluxes:

$$\begin{aligned} \theta_{i+\frac{1}{2},j} &= \langle \mu_{/}\mathbf{V}_{i+\frac{1}{2},j}, \mathbf{F}^{*}_{i+\frac{1}{2},j}\rangle - \mu_{/}\sigma_{i+\frac{1}{2},j} - \langle \mu_{/}\mathbf{V}_{i+\frac{1}{2},j}, Q_{i+\frac{1}{2},j}\Delta_{/}\mathbf{V}_{i+\frac{1}{2},j}\rangle, \\ \theta^{-}_{i+\frac{1}{2},j-\frac{1}{2}} &= \langle \mu_{/}\mathbf{V}_{i+\frac{1}{2},j-\frac{1}{2}}, \mathbf{F}^{-,*}_{i+\frac{1}{2},j-\frac{1}{2}}\rangle - \mu_{/}\sigma_{i+\frac{1}{2},j-\frac{1}{2}} - \langle \mu_{/}\mathbf{V}_{i+\frac{1}{2},j-\frac{1}{2}}, Q_{i+\frac{1}{2},j-\frac{1}{2}}\Delta_{/}\mathbf{V}_{i+\frac{1}{2},j\frac{1}{2}}\rangle. \end{aligned}$$

Note that the numerical entropy fluxes $\theta, \theta^{\pm}$ are consistent. Numerical entropy fluxes $\zeta, \zeta^{\pm}$ are defined analogously. Rest of terms in (3.6) can be manipulated in a similar manner. We obtain the following discrete entropy inequality:

$$\begin{aligned} \frac{d}{dt}(\eta_{i,j}) \leq &-\frac{1}{4\Delta x}\left(\Delta_{/}\theta^{+}_{i,j} + 2\Delta_x\theta_{i,j} + \Delta_{\backslash}\theta^{-}_{i,j}\right) - \frac{1}{4\Delta y}\left(\Delta_{/}\zeta^{+}_{i,j} + 2\Delta_y\zeta_{i,j} - \Delta_{\backslash}\zeta^{-}_{i,j}\right) \\ &- \frac{C}{4\Delta x}\left(\|\Delta_{/}\mathbf{V}_{i+\frac{1}{2},j+\frac{1}{2}}\|^2 + 2\|\Delta_x\mathbf{V}_{i+\frac{1}{2},j}\|^2 + \|\Delta_{\backslash}\mathbf{V}_{i+\frac{1}{2},j-\frac{1}{2}}\|^2\right) \\ &- \frac{C}{4\Delta y}\left(\|\Delta_{/}\mathbf{V}_{i+\frac{1}{2},j+\frac{1}{2}}\|^2 + 2\|\Delta_y\mathbf{V}_{i-\frac{1}{2},j}\|^2 + \|\Delta_{\backslash}\mathbf{V}_{i-\frac{1}{2},j+\frac{1}{2}}\|^2\right). \end{aligned} \tag{3.10}$$

Consistent numerical entropy fluxes imply that the discrete entropy inequality (3.10) is consistent with the entropy inequality (3.1) for the system (1.1).

Summing (3.10) over i, j, we obtain the entropy stability estimate (3.5). □

4. Scalar examples

We initiate the extensive numerical testing of the GMD schemes with scalar examples. The GMD schemes (2.5), (2.12) are in semi-discrete form and we use the standard forward Euler time stepping with first-order versions of the GMD scheme. Second-order strong stability preserving (SSP) Runge-Kutta method ([15]) is employed with the second-order semi-discrete version of the GMD scheme. The time step is determined by a standard CFL condition. All simulations reported here, are performed with a CFL number of 0.45. We test the following schemes:

SYM (SYM2)	first-order (second-order) symmetric GMD scheme (2.5) with forward Euler (Runge-Kutta) time stepping.
ISO (ISO2)	first-order (second-order) isotropic GMD scheme (2.12) with forward Euler (Runge-Kutta) time stepping.

The Rusanov flux (2.14) is used in all the above schemes. It is entropy stable, i.e, it satisfies (3.3), [35]. The SYM2 and ISO2 schemes are genuinely multi-dimensional extensions of the popular Kurganov-Tadmor central scheme, [18].

4.1. **Numerical Experiment 1: Scalar advection.**

Following [20], we consider the scalar advection equation

$$\begin{aligned} u_t + (a(x,y)u)_x + (b(x,y)u)_y &= 0 \\ a(x,y) = y, \quad b(x,y) &= -x, \end{aligned} \tag{4.1}$$

in the domain $[-2,2]\times[-2,2]$ with the initial data:

$$u(x,y,0) = \begin{cases} 1 & \text{if} \quad \{(-0.25 < x < 0.25) \cap (0.1 < y < 0.6)\}, \\ 1 - r/0.35 & \text{if} \quad r \equiv \sqrt{x^2 + (y+0.45)^2} < 0.35, \\ 0 & \text{otherwise.} \end{cases} \tag{4.2}$$

The velocity field in (4.1) is divergence free and the exact solution is a rotation of the data around the origin. The data contains both discontinuities and kinks and has circular as well as rectangular level sets. Hence, this problem serves as a good example to test the genuinely multi-dimensional properties of the schemes.

The approximate solutions at time $t = 2\pi$ on a uniform 200×200 mesh are plotted in figure 1. The figure shows that the first-order accurate SYM and ISO schemes smear the discontinuity. However, the geometry of the solution is intact and no multi-dimensional instabilities are observed. The second-order SYM2 and ISO2 schemes resolve the solution quite well. The discontinuity is captured very sharply. There is practically no difference between the symmetric and the isotropic schemes in this example. We also computed with the standard upwind flux and with the weighted version (2.6),(2.7) of the symmetric potential and the diagonal potential (2.10) and observed very very minor differences in the results.

4.2. **Numerical Experiment 2: Two-dimensional Burgers' equation.**

We consider the two dimensional Burgers' equation:

$$u_t + (\frac{1}{2}u^2)_x + (\frac{1}{2}u^2)_y = 0, \tag{4.3}$$

with the initial data (4.2) in the domain $[-2,2]\times[-2,2]$. The initial discontinuity and the initial kink evolve into a complex pattern of shocks and rarefactions. The approximate solutions on a 200×200 mesh at time $t = 0.5$ are shown in figure 2. The first-order SYM and ISO schemes are diffusive at this resolution. The multi-dimensional structures are resolved without any spurious waves. There are some differences between the SYM and ISO schemes. The SYM scheme appears to be less diffusive in this example. The second-order SYM2 and ISO2 schemes resolve the solution much more sharply. The results illustrate the non-linear stability of the GMD schemes and are comparable to those presented in [20].

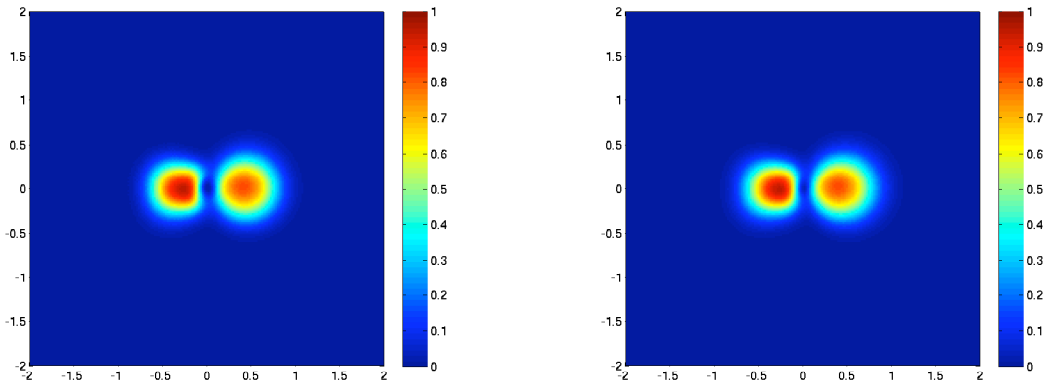

(a) SYM (b) ISO

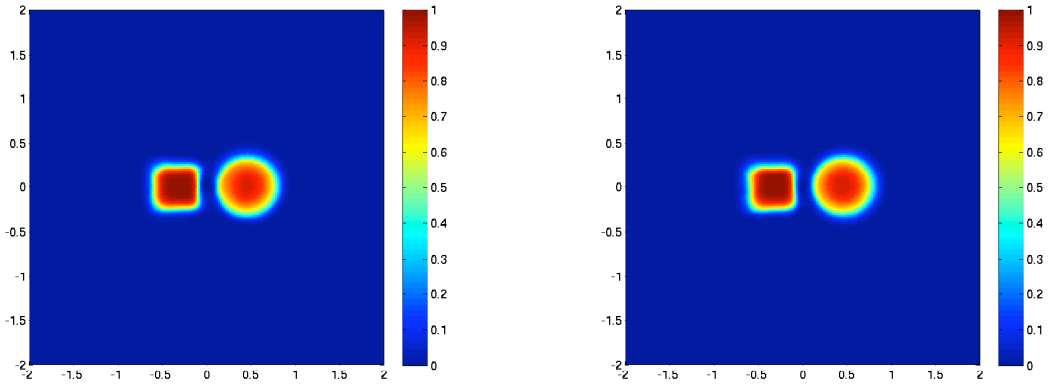

(c) SYM2 (d) ISO2

FIGURE 1. Approximate solutions u for numerical experiment 1 at $t = 2\pi$ on a 200×200 mesh computed with the GMD schemes.

5. The Euler equations

A prototypical example for the two dimensional system of hyperbolic conservation laws (1.1) are the Euler equations of gas dynamics:

$$\begin{aligned} \rho_t + (\rho u)_x + (\rho v)_y &= 0, \\ (\rho u)_t + (\rho u^2 + p)_x + (\rho uv)_y &= 0, \\ (\rho v)_t + (\rho uv)_x + (\rho v^2 + p)_y &= 0, \\ E_t + ((E+p)u)_x + ((E+p)v)_y &= 0, \end{aligned} \tag{5.1}$$

with ρ being the density of the gas, u, v are the velocity components in the x- and y-direction respectively and p and E are the pressure and the energy. The variables are related by an ideal gas equation of state:

$$E = \frac{p}{\gamma - 1} + \frac{1}{2}(\rho u^2 + \rho v^2), \tag{5.2}$$

where γ is the gas constant. The eigenvalues of the system, see [20], are

$$\{\lambda_1^x, \lambda_{2,3}^x, \lambda_4^x\} = \{u - c, u, u + c\}, \quad \{\lambda_1^y, \lambda_{2,3}^y, \lambda_4^y\} = \{v - c, v, v + c\},$$

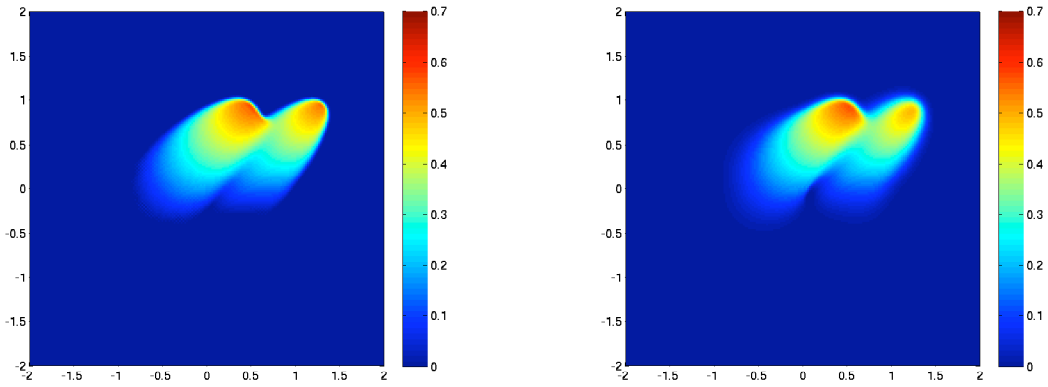

(a) SYM (b) ISO

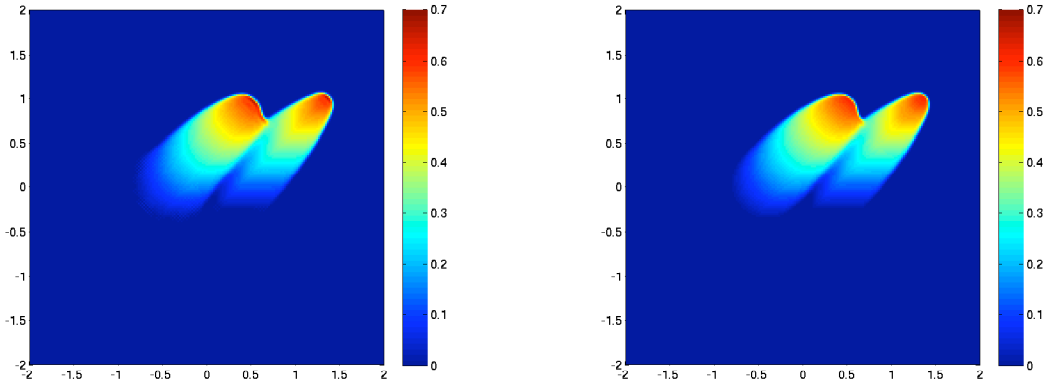

(c) SYM2 (d) ISO2

FIGURE 2. Approximate solutions u for numerical experiment 2 at $t = 0.5$ on a 200×200 mesh computed with the GMD schemes.

with $c = \sqrt{\frac{p}{\gamma\rho}}$ being the sound speed. The Rusanov flux (2.14) uses the above eigenvalues. The system is equipped with physical entropy $\eta = \log p - \gamma \log \rho$. The entropy stability estimate (3.5) holds for the isotropic ISO scheme.

5.1. **Numerical experiment 3.** The two-dimensional radially symmetric version of the standard Sod shock tube considers (5.1) with initial data:

$$\rho(x,y,0) = p(x,y,0) = \begin{cases} 1.0 & \text{if} \quad \sqrt{x^2+y^2} < 0.4, \\ 0.125 & \text{otherwise,} \end{cases} \tag{5.3}$$
$$u(x,y,0) = v(x,y,0) \equiv 0.$$

The initial radial discontinuity breaks into an outward propagating shock wave, a contact discontinuity and a rarefaction wave. The waves are radially symmetric and the standard finite volume scheme is known to be deficient, [20]. We consider the computational domain $[-2,2] \times [-2,2]$ and plot the approximate density at time $t = 0.2$, on a 200×200 mesh in figure 3. The first-order SYM and ISO schemes are diffusive but keep the circular features intact. In particular, the contact discontinuity is smeared out. However, no instabilities or grid-aligned spurious waves are observed. The second-order SYM2 scheme is much more accurate. There

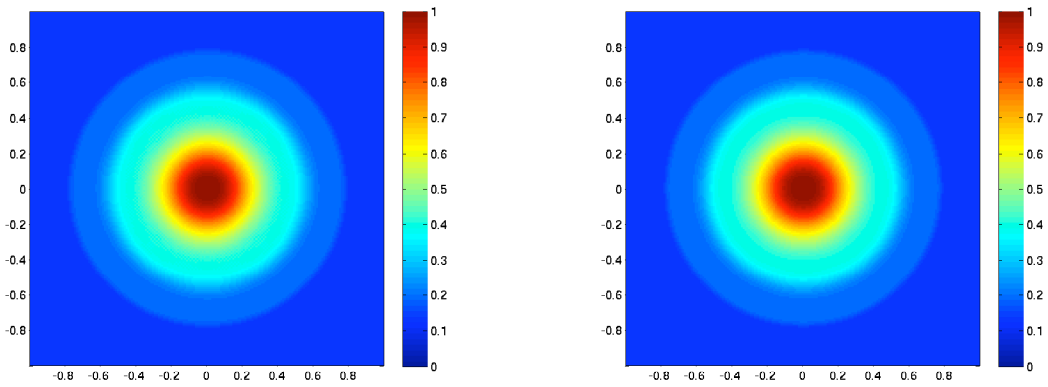

(a) SYM (b) ISO

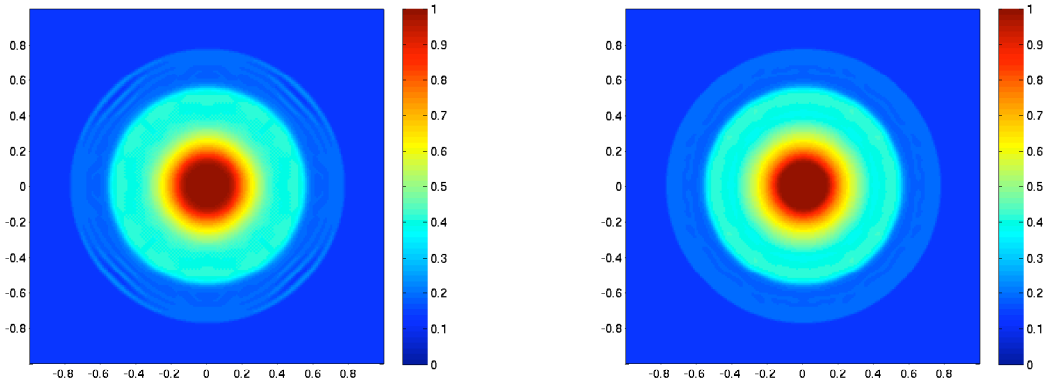

(c) SYM2 (d) ISO2

FIGURE 3. Approximate solutions of density for numerical experiment 3 at $t = 0.2$ on a 200×200 mesh computed with the GMD schemes.

are small oscillations at the outer shock, indicating that the scheme doesn't contain enough diffusion (similar examples were presented in [25]. The second-order ISO2 scheme results in no such oscillations and resolves the circular waves quite well. The accuracy is particularly evident at the contact discontinuity. The entropy stability of the ISO scheme might explain its robustness. The results are comparable to those presented in [23] and references therein.

5.2. **Numerical experiment 4.** As a second example for the Euler equations, we consider a benchmark test, [5, 12, 21, 23] and references therein. The two dimensional initial Riemann data is

$$\begin{aligned} \rho = 0.5313, \quad u = 0, \quad v = 0, \quad p = 0.4, \quad \text{if} \quad x > 0, y > 0, \\ \rho = 1.0, \quad u = 0, \quad v = 0.7276, \quad p = 1.0, \quad \text{if} \quad x > 0, y < 0, \\ \rho = 1.0, \quad u = 0.7276, \quad v = 0, \quad p = 1.0, \quad \text{if} \quad x < 0, y > 0, \\ \rho = 0.8, \quad u = 0, \quad v = 0, \quad p = 1.0, \quad \text{if} \quad x < 0, y < 0. \end{aligned} \tag{5.4}$$

The computational domain is $[-1, 1] \times [-1, 1]$. The exact solution consists of two forward moving shocks, two slip lines and a Mach reflection. There is a debate on whether standard finite volume schemes approximate the Mach reflection or a regular reflection, [12]. The approximate density at time $t = 0.5$, on a 200×200 mesh,

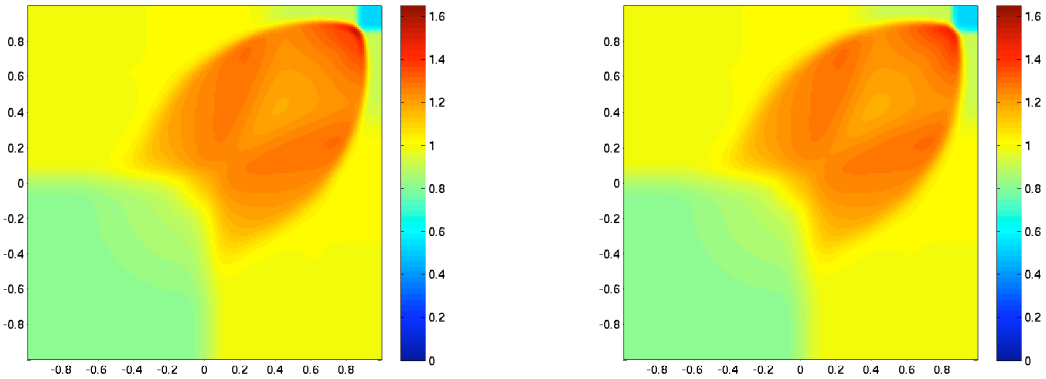

(a) SYM (b) ISO

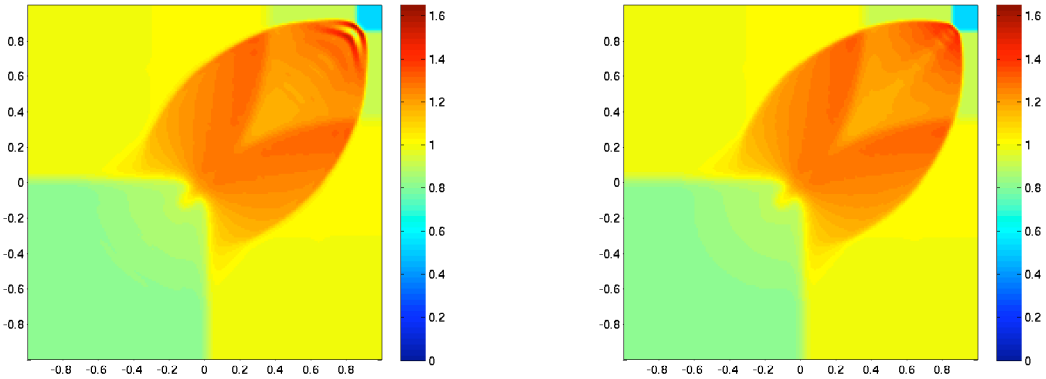

(c) SYM2 (d) ISO2

FIGURE 4. Approximate density for numerical experiment 4 at $t = 0.5$ on a 200×200 mesh computed with the GMD schemes.

is plotted in figure 4. The first-order SYM and ISO schemes are diffusive. This effect is particularly evident as we have scaled all the approximate solutions to the second-order results. Closer inspection reveals that the first-order schemes approximate the multi-dimensional waves well. The second-order ISO2 and SYM2 schemes have considerably better resolution, particularly at the slip lines and at the reflection. The SYM2 scheme has a slight overshoot at the top right corner, indicating the absence of sufficient diffusion. The ISO2 scheme is very stable and accurate. The results are comparable to the ones obtained in [12, 21, 23].

5.3. **Numerical experiment 5.** The Euler equations are considered with the two dimensional Riemann data:

$$
\begin{aligned}
\rho = 1.1, \quad u = 0, \quad v = 0, \quad p = 1.1, \quad &\text{if} \quad x > 0, y > 0, \\
\rho = 0.5065, \quad u = 0, \quad v = 0.8939, \quad p = 0.35, \quad &\text{if} \quad x > 0, y < 0, \\
\rho = 0.5065, \quad u = 0.8939, \quad v = 0, \quad p = 0.35, \quad &\text{if} \quad x < 0, y > 0, \\
\rho = 1.1, \quad u = 0.8939, \quad v = 0.8939, \quad p = 1.1, \quad &\text{if} \quad x < 0, y < 0,
\end{aligned}
\tag{5.5}
$$

The exact solution [23] consists of two forward moving shocks and two backward moving shocks. The computational domain is $[-1, 1] \times [-1, 1]$. The approximate density at time $t = 0.25$, on a 200×200 mesh, is plotted in figure 5. The results are very similar to the previous numerical experiment. The first-order ISO and SYM

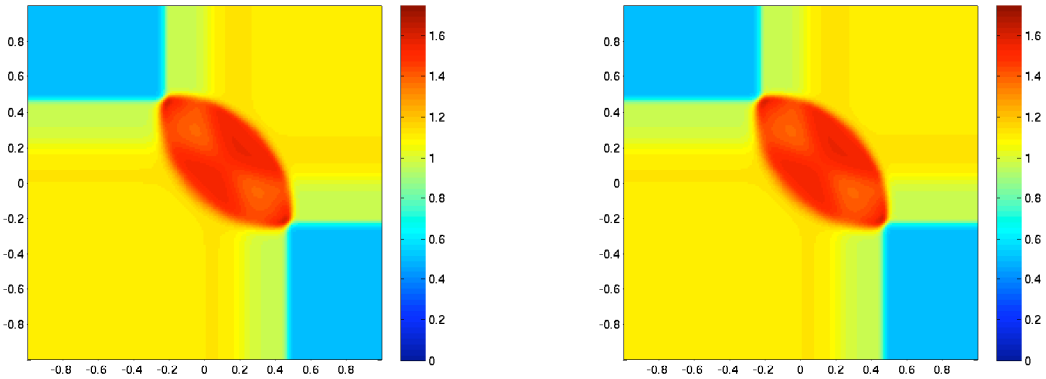

(a) SYM (b) ISO

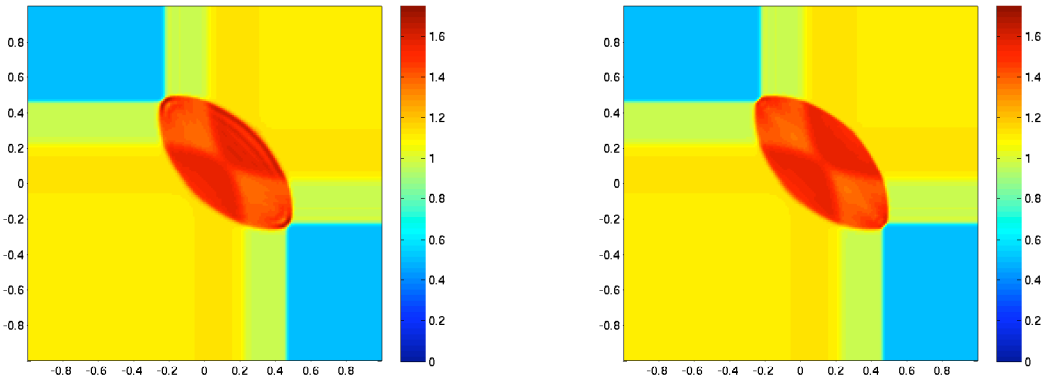

(c) SYM2 (d) ISO2

FIGURE 5. Approximate solutions of density for numerical experiment 5 at $t = 0.25$ on a 200×200.

schemes are diffusive but approximate the multi-dimensional waves qualitatively. The second-order schemes are much more accurate. The SYM2 scheme has a slight overshoot whereas the ISO2 scheme is very stable and has good resolution at the shocks as and at the reflection along the diagonal $x = -y$.

Remark 5.1. *The first-order SYM and ISO schemes are quite diffusive for the Euler equations. A possible reason is the use of the Rusanov flux* (2.14)*. It is well known that this flux is quite diffusive at first-order. Experiments with a more accurate flux like the Roe flux improved the quality of the results. However, we prefer the Rusanov flux as it is very cheap and doesn't require significant characteristic information about the system. Furthermore, the second-orders schemes, based on the Rusanov flux, are much more accurate.*

Remark 5.2. *The results presented here show that the GMD schemes are at least as robust and accurate as other GMD frameworks. The biggest advantage of our GMD schemes are their simplicity, ease of implementation and very low computational costs, when compared with other existing GMD frameworks. The black box nature of the GMD schemes is an added advantage.*

6. Constraint preserving schemes

Many interesting examples of of the conservation law (1.1) are augmented with an intrinsic constraint. Consider the grad advection:

$$\mathbf{U}_t + \nabla \mathbf{f}(\mathbf{x}, t, \mathbf{U}) = 0 \tag{6.1}$$

for any flux function $\mathbf{f}$. The constraint of interest is the vorticity $\omega = \text{curl}(\mathbf{U})$. Applying the curl operator on both sides of (6.1), we obtain

$$(\text{curl}(\mathbf{U}))_t \equiv 0.$$

A concrete example of a curl preserving equation is the system wave equation (1.3). We focus on the system wave equation for the rest of this section. It is well known, [27], that the standard finite volume scheme (1.2) may not preserve any discrete version of the vorticity. The symmetric GMD scheme (2.5) and isotropic GMD (2.12) for the system wave equation (1.3) are straightforward to define.

One would expect that the GMD schemes handle the vorticity constraint better than a standard finite volume scheme. This is indeed true and will be demonstrated in subsequent numerical experiments. However, we are unable to prove that either the symmetric GMD scheme (2.5) or the isotropic GMD scheme (2.12) preserves a discrete version of the vorticity. We need to choose a suitable form of the potential in-order to ensure constraint preservation.

The system wave equation (1.3) is endowed with a special property:

$$\mathbf{f}_2 = \mathbf{g}_3 = cp, \quad \mathbf{f}_3 = \mathbf{g}_2 = 0, \tag{6.2}$$

where h_i refers to the i-th component of the vector h. This structure of the fluxes ensures that the vorticity is preserved. We need to respect this special structure at the discrete level. This is done by choosing numerical potentials,

$$\phi_{i+\frac{1}{2},j+\frac{1}{2}} = \{(\phi_1)_{i+\frac{1}{2},j+\frac{1}{2}}, \xi_{i+\frac{1}{2},j+\frac{1}{2}}, 0\}, \quad \psi_{i+\frac{1}{2},j+\frac{1}{2}} = \{(\psi_1)_{i+\frac{1}{2},j+\frac{1}{2}}, 0, \xi_{i+\frac{1}{2},j+\frac{1}{2}}\}. \tag{6.3}$$

The potentials ϕ_1, ψ_1 have to be consistent with the fluxes $\mathbf{f}_1 = cu$ and $\mathbf{g}_1 = cv$ respectively. A simple choice of these potentials are the symmetric potentials (2.4), based on averaging the first component of the Rusanov flux (2.14).

The potential ξ needs to be consistent with $\mathbf{f}_2 = \mathbf{g}_3 = cp$. Following the recent paper [25], we use the symmetric potential:

$$\xi_{i+\frac{1}{2},j+\frac{1}{2}} = \frac{1}{4}((\mathbf{F}_2)_{i+\frac{1}{2},j} + (\mathbf{F}_2)_{i+\frac{1}{2},j+1} + (\mathbf{G}_3)_{i,j+\frac{1}{2}} + (\mathbf{G}_3)_{i+1,j+\frac{1}{2}}). \tag{6.4}$$

The numerical fluxes $\mathbf{F}_2, \mathbf{G}_3$ are the corresponding components of the Rusanov flux (2.14). Combining the above ingredients (see the description of (2.3)), the resulting potential based schemes reads as

$$\begin{aligned} \frac{d}{dt} p_{i,j} &= -\delta_x \mu_y (\phi_1)_{i,j} - \delta_y \mu_x (\psi_1)_{i,j}, \\ \frac{d}{dt} u_{i,j} &= -\delta_x \mu_y \xi_{i,j}, \\ \frac{d}{dt} v_{i,j} &= -\delta_y \mu_x \xi_{i,j}. \end{aligned} \tag{6.5}$$

The above scheme is a specific form of the potential based scheme (2.3). It is consistent and conservative. The constraint preserving abilities of the schemes are stated below:

Lemma 6.1. *Let $u_{i,j}, v_{i,j}$ be the approximate velocities for the system wave equation* (1.3)*, computed with the potential based scheme* (6.5)*. Then their discrete vorticity ω^*, given by*

$$\omega^*_{i,j} = \frac{1}{\Delta x}(\mu_y \delta_x v_{i,j}) - \frac{1}{\Delta y}(\mu_x \delta_y u_{i,j}). \tag{6.6}$$

is preserved in time:

$$\frac{d}{dt}(\omega^*_{i,j}) \equiv 0, \quad \forall i, j.$$

Verification of (6.6) is straightforward as the difference operators δ_x, δ_y and the averaging operators μ_x, μ_y commute with each other. Applying the discrete vorticity operator ω^* to the numerical solution of (6.5), we find

$$\frac{d}{dt}\omega^*_{i,j} = -(\mu_y\delta_x\delta_y\mu_x - \mu_x\delta_y\delta_x\mu_y)\xi_{i,j} \equiv 0.$$

Remark 6.1. *One approach in designing constraint preserving schemes is to satisfy that constraint* approximately*: for example, the discrete statement of the vorticity constraint* (1.4) *could be interpreted as a second-order approximation of the differential vorticity,*

$$\omega^*_{i,j} = \omega(x_i, y_j) + \mathcal{O}(\Delta x^2 + \Delta y^2).$$

This, however, require the smoothness of the underlying solution. Instead, a key feature of constraint preserving schemes based on numerical potentials is that they satisfy exactly *a discrete constraint, so that their numerical solution remains on a discrete sub-manifold, independent of the underlying smoothness.*

A potential based GMD scheme preserving discrete divergence was described in [25].

7. System wave equation: Numerical experiments

We test the symmetric GMD scheme (2.5), isotropic GMD scheme (2.12) and the constraint preserving GMD scheme (6.5) on the system wave equation (1.3). The four GMD schemes: SYM, ISO, SYM2 and ISO2 are tested along with a first-order constraint preserving scheme (6.5) (with forward Euler time stepping). The first-order scheme (6.5) is extended to second order of accuracy by the reconstruction procedure outlined in Section 2. The first- and second-order versions of the constraint preserving schemes are termed SCP and SCP2 respectively.

7.1. **Numerical experiment** 6**:** Following [22, 24], we consider the system wave equation (1.3) in the domain $[-2, 2] \times [-2, 2]$ with the initial data:

$$\begin{aligned} p(x, y, 0) &= -e^{-15(x^2+y^2)}, \\ u(x, y, 0) = v(x, y, 0) &\equiv 0. \end{aligned} \tag{7.1}$$

The wave speed c in (1.3) is set to one. The initial data is smooth and the exact solution consists of smooth circular waves. We compute on a uniform 200×200 mesh and plot the approximate pressure p at time $t = 0.8$ in figure 6. The figure shows that the first-order SYM, ISO and SCP schemes resolve the circular waves with some diffusion. The GMD structure is resolved without any noticeable instabilities. The second-order SYM2, ISO2 and SCP2 schemes are much more accurate. The circular waves are resolved quite sharply.

The initial data has zero vorticity and the vorticity should remain zero for all time. We compute errors in L^1 for the discrete vorticity (6.6) and show the results in Table 1. The SYM scheme doesn't preserve the discrete vorticity. However, the vorticity errors are small and converge to zero as the mesh is refined. A similar trend is observed with the second-order SYM2 scheme. The constraint preserving SCP and SCP2 scheme lead to very low vorticity errors. The errors are due to boundary effects as no special vorticity cleaning is used at the boundaries. As expected, the constraint preserving SCP and SCP2 schemes preserve vorticity to machine precision on fine meshes. Surprisingly, the ISO scheme also preserves vorticity. This may be due to its isotropic nature. Its second-order version, the ISO2 scheme doesn't preserve discrete vorticity.

M	SYM	ISO	SCP	SYM2	ISO2	SCP2
50	9.3e-2	1.5e-6	3.5e-7	6.7e-2	4.2e-2	1.0 e-8
100	2.8e-2	8.5e-9	1.3e-9	2.4e-2	1.6e-2	1.8e-11
200	7.9e-4	9.4e-11	1.3e-11	9.5e-4	6.0e-4	2.2e-13
400	2.1e-4	3.0e-12	4.5e-13	1.6e-4	1.2e-4	2.6e-16

Table 1. Vorticity errors in L^1 for numerical experiment 6.

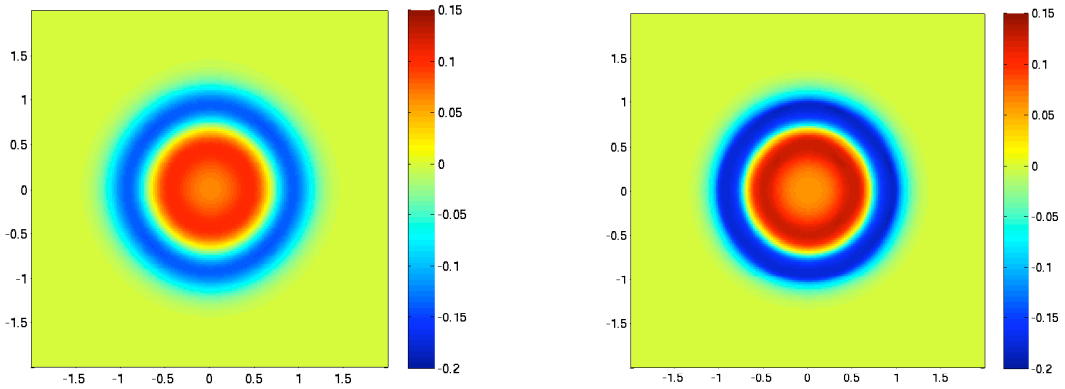

(a) SYM

(b) SYM2

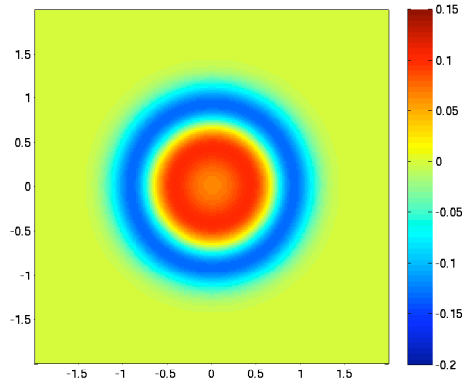

(c) ISO

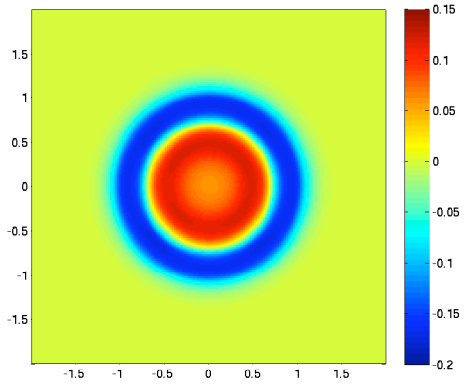

(d) ISO2

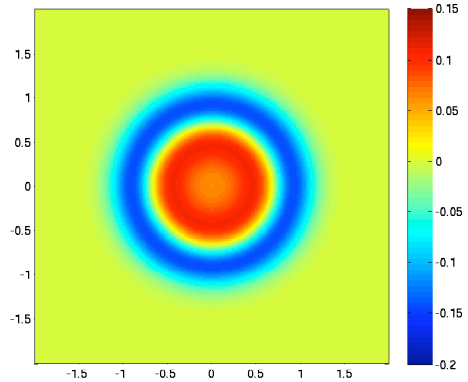

(e) SCP

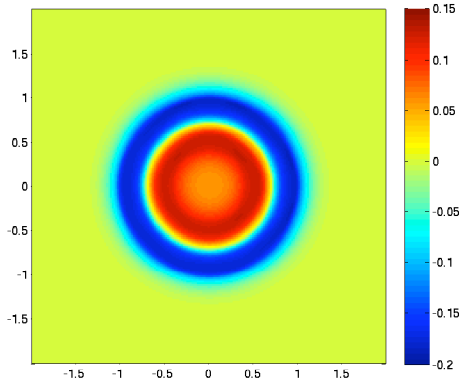

(f) SCP2

FIGURE 6. Approximate solutions p for numerical experiment 6 at $t = 0.25$ on a 200×200 mesh. Left column: first-order schemes. Right column: second-order schemes

7.2. **Numerical experiment 7:** We conclude the discussion on the system wave equation by consider the following discontinuous initial data ([22]):

$$p(x,y,0) = \begin{cases} 1 & \text{if} \quad \sqrt{x^2+y^2} \leq 0.4 \\ 0 & \text{otherwise,} \end{cases} \tag{7.2}$$
$$u(x,y,0) = v(x,y,0) \equiv 0.$$

The approximate pressures, on a uniform 200×200 mesh, at time $t = 0.5$ are shown in figure 7. The results are very similar to the previous numerical experiment. The first-order schemes diffuse the shock but the geometric properties of the solution are respected. The second-order schemes are more accurate and resolve the circular discontinuities sharply. There are very minor differences between the constraint preserving SCP scheme and the standard GMD schemes. Table 2 displays the errors in vorticity. All the first-order schemes preserve vorticity to machine precision. This is to expected from the constraint preserving SCP scheme but the SYM and ISO schemes also preserve vorticity to machine precision. However, the second-order SYM2 and ISO2 schemes lead to vorticity errors.

M	SYM	ISO	SCP	SYM2	ISO2	SCP2
50	3.9e-16	3.2e-16	2.5e-16	1.1e-2	4.0e-2	1.0 e-16
100	3.6e-16	3.0e-16	1.3e-16	4.1e-3	4.1e-2	1.8e-17
200	3.6e-16	3.0e-16	3.1e-17	2.0e-4	1.7e-4	1.3e-17
400	3.0e-16	3.0e-16	1.5e-17	7.6e-5	1.2e-5	1.6e-17

TABLE 2. Vorticity errors in L^1 for numerical experiment 7.

8. Conclusion

Standard finite volume schemes (1.2) for the system of conservation laws (1.1) are known to be deficient in resolving genuinely multi-dimensional waves. Many strategies are proposed to address this issue. Most of them are complicated and computationally expensive.

We present an alternative framework for designing genuinely multi-dimensional (GMD) schemes. The building blocks are the standard finite volume fluxes. The scheme is based on vertex centered *numerical potentials*. The use of potentials incorporates transverse information in each direction and endows GMD structure on the scheme. The family of potential based GMD schemes (2.3) is very rich. Any standard finite volume flux can define the potential. Consequently, the approach is extremely general. A related scheme is the isotropic GMD scheme (2.12). Higher order accuracy is obtained by employing non-oscillatory piecewise polynomial reconstructions. The use of Rusanov flux (2.14) and piecewise bilinear reconstructions leads to a GMD extension of the popular central schemes of Kurganov and Tadmor, [18].

The isotropic GMD scheme is proved to be entropy stable if its building block fluxes are entropy stable. Numerical experiments involving scalar conservation laws and Euler equations illustrate the robustness and computational efficiency of this new approach. The numerical results are comparable to those obtained with other GMD frameworks. The principal advantages of the new approach are its simplicity and low computational cost. The entire framework can be considered as a *black box* GMD solver for systems of hyperbolic conservation laws.

Another advantage of this approach is its ability to deal with conservation laws with intrinsic constraints. A suitable choice of potential leads to a GMD scheme, that preserves a discrete version of the vorticity (or divergence). Numerical experiments with the system wave equation demonstrate the robustness of the constraint preserving GMD schemes.

The next paper [26] in this series deals with GMD schemes for the ideal MHD equations. Forthcoming papers consider third and even higher order GMD schemes and extending the Cartesian GMD schemes of this paper to unstructured grids.

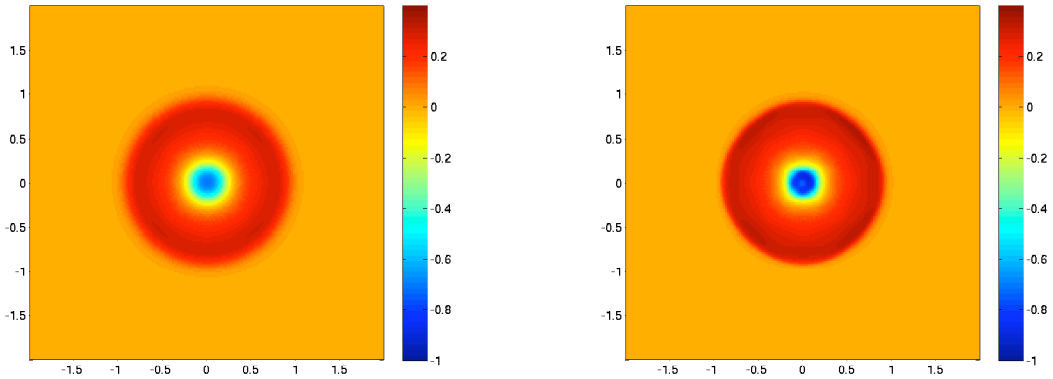

(a) SYM

(b) SYM2

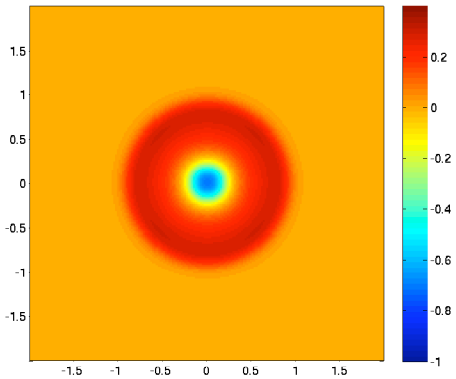

(c) ISO

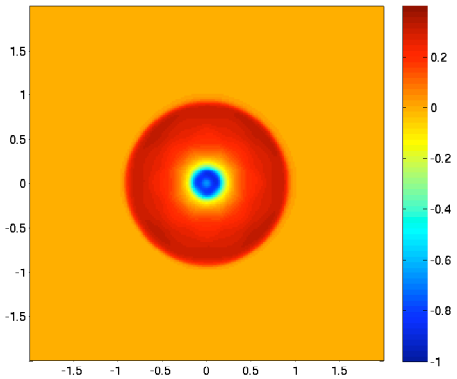

(d) ISO2

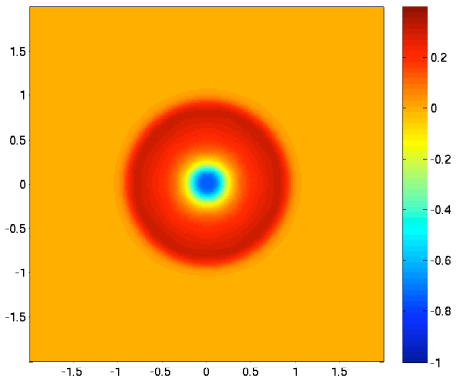

(e) SCP

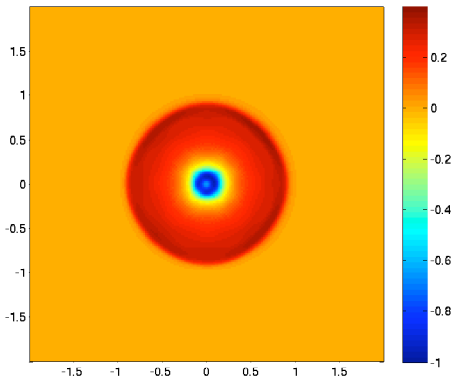

(f) SCP2

FIGURE 7. Approximate solutions of p for numerical experiment 7 at $t = 0.5$ on a 200×200 mesh. Left: first-order schemes. Right: second-order schemes.

References

[1] R. Abgrall and P. L. Roe. High-order fluctuation schemes on triangular meshes. *SIAM J. sci. comput.,* 198, 3 -36, 2003.

[2] J. Bálbas , E. Tadmor and C. C. Wu. Non-oscillatory central schemes for one and two-dimensional magnetohydrodynamics I. *J. Comp. Phys.,* 201 (1), 261-285, 2004.

[3] D. S. Balsara and D. Spicer. A staggered mesh algorithm using high order Godunov fluxes to ensure solenoidal magnetic fields in magnetohydrodynamic simulations. *J. Comp. Phys.*, 149(2):270-292, 1999.

[4] J. U. Brackbill and D. C. Barnes. The effect of nonzero Div$B$ on the numerical solution of the magnetohydrodynamic equations. *J. Comp. Phys.*, 35:426-430, 1980.

[5] M. Brio, A. R. Zakharian, and G. M. Webb. Two-dimensional Riemann solver for Euler equations of gas dynamics. *J. Comp. Phys.,* 167 (1):177-195, 2001.

[6] A. J. Chorin. Numerical solutions of the Navier-Stokes equations. *Math. Comp.*, 22, 745-762, 1968.

[7] P. Colella. Multi-dimensional upwind methods for hyperbolic conservation laws. *J. Comp. Phys.,* 87, 171-200, 1990.

[8] C. Dafermos. *Hyperbolic conservation laws in continuum physics.* Springer, Berlin, 2000.

[9] W. Dai and P. R. Woodward. A simple finite difference scheme for multi-dimensional magnetohydrodynamic equations. *J. Comp. Phys.*, 142(2):331-369, 1998.

[10] H. Deconnik, P. L. Roe and R. Struijs. A multi-dimensional generalization of Roe's flux difference splitter for Euler equations. *Comput. Fluids*, 22, 215, 1993.

[11] C. Evans and J. F. Hawley. Simulation of magnetohydrodynamic flow: a constrained transport method. *Astrophys. J.*, 332:659, 1998.

[12] M. Fey. Multi-dimensional upwingding.(I) The method of transport for solving the Euler equations. *J. Comp. Phys.,* 143(1): 159-180, 1998.

[13] M. Fey. Multi-dimensional upwingding.(II) Decomposition of Euler equations into advection equations. *J. Comp. Phys.,* 143(1): 181-199, 1998.

[14] F. Fuchs, A. D. McMurry, S. Mishra, N. H. Risebro and K. Waagan. Approximate Riemann solver based high order finite volume schemes for the Godunov-Powell form of the ideal MHD equations in multi dimensions. *Preprint,* 2009.

[15] S. Gottlieb, C. W. Shu and E. Tadmor. High order time discretizations with strong stability property. *SIAM. Review,* 43, 2001, 89 - 112.

[16] A. Harten, B. Engquist, S. Osher and S. R. Chakravarty. Uniformly high order accurate essentially non-oscillatory schemes. *J. Comput. Phys.*, 1987, 231-303.

[17] R. Jeltsch and M. Torrilhon. On curl preserving finite volume discretizations of the shallow water equations. *BIT*, 46, 2006, suppl.

[18] A. Kurganov and E. Tadmor. New high resolution central schemes for non-linear conservation laws and convection-diffusion equations. *J. Comput. Phys*, 160(1), 241-282, 2000.

[19] A. Kurganov, S. Noelle and G. Petrova. Semi-discrete central upwind schemes for hyperbolic conservation laws and Hamilton-Jacobi equations. *SIAM J. Sci. comput.,* 23(3), 707 - 740, 2001.

[20] R. J. LeVeque. Finite volume methods for hyperbolic problems. *Cambridge university press,* Cambridge, 2002.

[21] R. J. LeVeque. Wave propagation algorithms for multi-dimensional hyperbolic systems, *J. Comp. Phys.,* 131, 327-353, 1997.

[22] M. Lukacova-Medvidova, K. W. Morton and G. Warnecke. Evolution Galerkin methods for Hyperbolic systems in two space dimensions. *Math. Comp.,* 69 (232), 1355 - 1384, 2000.

[23] M. Lukacova-Medvidova, J. Saibertova and G. Warnecke. Finite volume evolution Galerkin methods for Non-linear hyperbolic systems. *J. Comp. Phys.,* 183, 533 - 562, 2003.

[24] M. Lukacova-Medvidova and J. Saibertova. Finite volume schemes for multi-dimensional hyperbolic systems based on use of bi-characteristics. *Appl. Math.,* 51 (3), 205 - 228, 2006.

[25] S. Mishra and E. Tadmor, Constraint preserving schemes using potential-based fluxes. I. Multi-dimensional transport equations. *Preprint,* 2009.

[26] S. Mishra and E. Tadmor, Constraint preserving schemes using potential-based fluxes. III. Divergence preserving central schemes for the MHD equations. *Preprint,* 2009.

[27] K. W. Morton and P. L. Roe. Vorticity preserving Lax-Wendroff type schemes for the system wave equation. *SIAM. J. Sci. Comput.,* 23 (1), 2001, 170-192.

[28] H. Nishikawa and P. L. Roe. Towards high-order fluctuation-splitting schemes for Navier-Stokes equations. *AIAA paper*, 2005-5244, 2005.

[29] S. Noelle. The MOT-ICE: A new high-resolution wave propagation algorithm for multi-dimensional systems of conservation laws based on Fey's method of transport. *J. Comp. Phys.,* 164, 283 - 334, 2000.

[30] K. G. Powell. An approximate Riemann solver for magneto-hydro dynamics (that works in more than one space dimension). Technical report, 94 -24, ICASE, Langley, VA, 1994.

[31] D. S. Ryu, F. Miniati, T. W. Jones and A. Frank. A divergence free upwind code for multidimensional magnetohydrodynamic flows. *Astrophys. J.*, 509(1):244-255, 1998.

[32] C. W. Shu and S. Osher. Efficient implementation of essentially non-oscillatory schemes - II, *J. Comput. Phys.*, 83, 1989, 32 - 78.w

[33] E. Tadmor. Numerical viscosity and entropy conditions for conservative difference schemes. *Math. Comp.*, 43 (168), 369 -381, 1984.

[34] E. Tadmor. The numerical viscosity of entropy stable schemes for systems of conservation laws, I. *Math. Comp.,* 49, 91-103, 1987.
[35] E. Tadmor. Entropy stability theory for difference approximations of nonlinear conservation laws and related time-dependent problems. *Act. Numerica.,* 451-512, 2004.
[36] E. Tadmor. Approximate solutions of nonlinear conservation laws. *Advanced Numerical approximations of Nonlinear Hyperbolic equations, A. Quarteroni ed.*, Lecture notes in Mathematics, Springer Verlag (1998), 1-149.
[37] M. Torrilhon. Locally divergence preserving upwind finite volume schemes for magneto-hydro dynamics. *SIAM. J. Sci. Comp.*, 26 (4), 1166-1191, 2005.
[38] M. Torrilhon and M. Fey. Constraint-preserving upwind methods for multidimensional advection equations. *SIAM. J. Num. Anal.*, 42(4):1694-1728, 2004.
[39] G. Toth. The Div$B = 0$ constraint in shock capturing magnetohydrodynamics codes. *J. Comp. Phys.*,161:605-652, 2000.

(Siddhartha Mishra)
SAM, D-MATH
ETH Zürich
HG. G. 57.2, Rämistrasse 101, Zürich, Switzerland
E-mail address: smishra@sam.math.ethz.ch

(Eitan Tadmor)
Department of Mathematics
Center of Scientific Computation and Mathematical Modeling (CSCAMM)
Institute for Physical sciences and Technology (IPST)
University of Maryland
MD 20741-4015, USA
E-mail address: tadmor@cscamm.umd.edu

Research Reports

No.	Authors/Title
09-32	*S. Mishra, E. Tadmor* Constraint preserving schemes using potential-based fluxes. II. Genuinely multi-dimensional central schemes for systems of conservation laws
09-31	*S. Mishra, E. Tadmor* Constraint preserving schemes using potential-based fluxes. I. Multidimensional transport equations
09-30	*D. Braess, S. Sauter, C. Schwab* On the justification of plate models
09-29	*D. Schötzau, C. Schwab, T. Wihler* *hp*-dGFEM for second-order elliptic problems in polyhedra. II: Exponential convergence
09-28	*D. Schötzau, C. Schwab, T. Wihler* *hp*-dGFEM for second-order elliptic problems in polyhedra. I: Stability and quasioptimality on geometric meshes
09-27	*A. Moiola, R. Hiptmair, I. Perugia* Approximation by plane waves
09-26	*M. Karow, E. Kokiopoulou, D. Kressner* On the computation of structured singular values and pseudospectra
09-25	*M. Durán, M. Guarini, C.F. Jerez-Hanckes* Hybrid FEM/BEM modeling of finite-sized photonic crystals for semiconductor laser beams
09-24	*A. Bespalov, N. Heuer, R. Hiptmair* Convergence of the natural *hp*-BEM for the electric field integral equation on polyhedral surfaces
09-23	*R. Hiptmair, J. Li, J. Zou* Real interpolation of spaces of differential forms
09-22	*R. Hiptmair, J. Li, J. Zou* Universal extension for Sobolev spaces of differential forms and applications
09-21	*T. Betcke, D. Kressner* Perturbation, computation and refinement of invariant pairs for matrix polynomials
09-20	*R. Hiptmair, A. Moiola, I. Perugia* Plane wave discontinuous Galerkin methods for the 2D Helmholtz equation: analysis of the p–version